Processing/microstructure relationships in melt compounded polyamide 6 with different molecular weights: Effect of screw speed and viscosity ratio

Received: 10 January 2025 | Revised: 18 February 2025 | Accepted: 19 February 2025

DOI: 10.1002/pen.27165

RESEARCH ARTICLE

POLYMER ENGINEERING AND SCIENCE WILEY

Processing/microstructure relationships in melt compounded polyamide 6 with different molecular weights: Effect of screw speed and viscosity ratio

Fulvia Cravero[1,2] | **Rossella Arrigo**[1,2] | **Alberto Frache**[1,2]

[1]Department of Applied Science and Technology, Polytechnic of Torino, Alessandria, Italy

[2]INSTM Local Unit, Florence, Italy

Correspondence
Rossella Arrigo, Department of Applied Science and Technology, Polytechnic of Torino, Viale Teresa Michel, 5, 15121 Alessandria, Italy.
Email: rossella.arrigo@polito.it

Abstract

In this work, the relationships between the processing parameters and the microstructure in melt-compounded polyamide 6 (PA6) are investigated. To this aim, two PA6 having different viscosities are processed in a twin-screw extruder at two different screw speeds (150 or 300 rpm) and characterized through rheological and thermal analyses. Furthermore, the thermo-mechanical field along the screw is simulated using Ludovic® software, and the obtained results in terms of shear rate, residence time, and actual temperature are exploited to disclose interesting processing/microstructure relationships. In particular, the antagonistic role of the flow-induced crystallization (FIC) and memory effect in governing the final microstructure is assessed. Specifically, for high screw speed and viscosity, FIC outweighs the memory effect due to the higher shear rate and temperature experienced by the material during processing. Besides, the dominant influence of FIC over the memory effect is found to be responsible for the higher overall crystallinity and α/γ content observed for the materials processed at 300 rpm. Finally, the same analyses are performed on blends containing different relative contents of the two PA6, demonstrating the interdependency of the screw speed and viscosity effects on the resulting microstructure.

Highlights

- Processing parameters/microstructurerelationships for PA6 are investigated.
- PA6 with different viscosities wasmelt compounded using two screw speeds.
- Shear rate, temperature and residencetime during the processing were simulated.
- Screw speed and viscosity affectflow-induced crystallization and memory effect.
- High screw speed and viscositypromoted FIC over the memory effect.

KEYWORDS
flow-induced crystallization, melt compounding, memory effect, PA6, processing parameters

1 | INTRODUCTION

Aliphatic polyamides (PAs) are well known for the thermo-mechanical properties determining their importance as engineering polymers exploited in sports, automotive, aerospace applications, and health tech.[1–6] However, even if they are largely exploited and studied, some issues are not yet clear and require more investigation; specifically, the relationships between the processing conditions and the resulting microstructure are not completely understood.

In fact, the microstructure of polyamide-based systems is the result of different complex phenomena concurrently occurring during their solidification and crystallization from the molten state, which are influenced by the thermo-mechanical field undergone by the material during the melt processing.[1,2] For instance, the presence of the H-bonding between the macromolecules is responsible for the so-called memory effect.[1,7–9] This phenomenon is the partial retention of the chains' organization in the molten state owing to the presence of intermolecular H-bonding between the amide groups.[2,8,10–14] In fact, despite this kind of interaction weakening as the temperature increases, it was observed that in the molten state the H-bonding is in a dynamic temperature-dependent equilibrium. Specifically, they are statistically bonded and broken at any moment with the achievement of a constant average number of free NH groups, while certain conditions are needed to completely remove the bonding.[2,8,15,16] Besides, it is important to point out that, since the memory effect is strongly related to the presence of the intermolecular H-bonding, the presence of entanglement was also assessed to play an important role in favoring it.[17]

A further phenomenon related to the presence of H-bonding in molten PAs is the shear-induced or flow-induced crystallization (FIC).[2,7,18,19] FIC is a multi-order coupling process in which the flow of the molten polymer determines the evolution of the microstructure. In particular, the final morphology results from the competition between the chain relaxation and the crystallization kinetic, possibly resulting also in the formation of hierarchical crystalline structures. This phenomenon is a nonequilibrium thermodynamic phase transition depending on the intrachain conformation, the interchain orientation, and the density fluctuations in the melt.[19–21] In fact, in order to understand the evolution of the system, different theories (such as "flow-induced coil-helix transition" theory,[22] "conformation-density coupling for phase separation" theory,[23] "isotropic-nematic transition" theory[24,25] and the "entropic reduction-energy change" model[26]) tried to couple two of the aforementioned phenomena. However, none of them is exhaustive in modeling the final microstructure due to lack in describing the thermodynamic determining the intermediate morphologies of the macromolecules induced by the flow.[19] On the other hand, the role of the H-bonding in FIC was highlighted as promoting the retention of the improved ordered structure reached owing to the application of the shear rate.[7] From a general point of view, it has been observed that, for polymers experiencing FIC and memory effect, the final microstructure is determined by the interplay of the two phenomena. In particular, it has been shown that the flow affects the size distribution of the ordered clusters in the molten state retained owing to the H-bonding.[27–29]

Therefore, considering the above-described impact of the temperature on the H-bonding strength and its role in assisting the stability of the more ordered macromolecular morphology resulting from the application of the shear, it is clear that the resulting microstructure of PAs is strongly impacted by the thermo-mechanical field faced by the material during processing.

Lastly, it has to be taken into account that PAs are polymorphic materials.[1,7,9,11,30–32] Hence, depending on the thermal history, several crystal structures can be obtained. For instance, in polyamide 6 (PA6), the two more common crystalline phases are α and γ.[2,30,33–37] In both cases, the chains are organized in parallel sheet-like planes, forming a monoclinic crystal. However, in the α phase, the macromolecules are fully extended in a zig-zag conformation in which the H-bonding occurs between the antiparallel chains, while in the γ phase the amide groups are rotated by about 60°, and the parallel macromolecules are constrained. This results in melting temperatures of 223 and 215°C, respectively.

Nonetheless, as already remarked, a poor knowledge of the processing parameters—microstructure relationships affects this family of polymers, and this results in unsatisfactory control over the tunability of the final properties.[11,38–40] This is mostly due to the presence of H-bonding and its consequences. In fact, the impact of the thermic or mechanical fields on memory effect, FIC, and polymorphism was deeply studied in the last decades.[7,10,15,31,34] However, the effects of these different phenomena are usually studied separately. For instance,

the effect of the temperature and cooling rates on the crystallization is typically evaluated through DSC,[30,33–35,41] while the impact of the shear is usually monitored via isothermal rheological tests.[18,42] As a result, the combined effect of the thermo-mechanical field when PAs are melt processed is not yet fully understood. However, recently research shifted to real processing equipment, so as to take into consideration the actual conditions that the polymers undergo during processing. In this context, Skorupska et al.[43,44] assessed the effect of the processing parameters in cold hydrostatic extrusion on the final microstructure of PA6. In particular, it emerged that an increase of the extrusion pressure in the range of 103–262 MPa promotes the orientation of the macromolecules, inducing a higher content of α crystalline phase and a concurrent enhancement of the tensile strength.[9,45] However, to the best of the authors knowledge, no systematic study on the impact of the processing conditions on the final microstructure of PAs is available yet.

Nevertheless, it is a very important issue, as the processing conditions and the resulting microstructure have a strong influence on the final mechanical behavior of this class of polymers. In this context, it has been reported in the literature that a higher content of γ crystalline phase promotes a more ductile behavior compared to a PA6 composed mainly of α crystals.[46,47]

Considering all the aforementioned aspects, the present study aims to bring new knowledge toward the understanding of the effect of the processing parameters during twin-screw extrusion (especially screw speed) on the final microstructure of PA6.

Furthermore, it should be considered that the macromolecular parameters of the material (such as molecular weight [M_W] or M_W distribution) also play a fundamental role in determining its microstructure. For instance, it is well known that the achievement of a high crystallinity in polymers characterized by a monomodal M_W distribution is limited by the high M_W of the chains. This limitation can be overcome through the synthesis of ad hoc macromolecules characterized by a bimodal M_W distribution.[48,49] On the other hand, a cheaper, more versatile, and easily industrially scalable alternative is represented by melt blending, which allows tailoring the macromolecular characteristics by exploiting the compounding of two or more polymers having different M_W. For this reason, this method is often employed for the production of bimodal M_W materials.[48,50–52] On the other hand, in the case of PAs, this approach has not yet been greatly deepened, and the studies usually refer to the effect of the presence of copolymers in the blends.[52–54] Therefore, in this work, two different PA6 characterized by different M_W (hence, viscosity) were exploited, also considering melt-compounded blends containing different relative contents of the two polymers.

Besides, Ludovic® software was exploited to model the evolution of the temperature, shear rate, and residence time faced by the materials along the screws. The results obtained through the simulations were then related to the rheological behavior and the crystalline structure of the processed materials, taking into consideration the role of both the memory effect and FIC with the variation of the parameters. In these terms, the possibility of modulating the material microstructure was assessed, bringing new knowledge toward the understanding of processing—microstructure relationships in PAs.

2 | EXPERIMENTAL SECTION

2.1 | Materials

In this study, two PA6 with different M_Ws were used. Both polymers are commercially available and were provided by RADICI Group:

- Radipol S24, exploited as a low viscosity polymer and named LV. The relative viscosity (MAR01 method) is 2.4 dL/g.
- Radipol S40P, selected as a high viscosity polymer and named HV, has a relative viscosity (MAR01 method) of 4.0 dL/g.

2.2 | Methods

2.2.1 | Processing

A ThermoFisher Process 11 (Waltham, MA, USA) twin-screw extruder (diameter = 11 mm, $L/D = 40$, barrel length = 440 mm) was used. It is equipped with eight independent heating zones, seven internal and one external corresponding to the die. The used screw profile is reported in Figure 1. The screw elements in terms of length and corresponding codes are reported in Table 1. The selected screw configuration presents three kneading blocks and four conveying sections. The kneading blocks are characterized by different stagger angles. Specifically, the first one consists of three sets of elements at 30°, 60°, and 90°, in order to plasticize the polymer. Then, the second kneading section with the constant angle of 60° is present. Lastly, the third kneading zone consists of a section having stagger angles of 60° and 90°.

The conveying elements are identified by the letter "C" and the number corresponds to the sequential position starting from the hopper. For instance, "C2" refers to

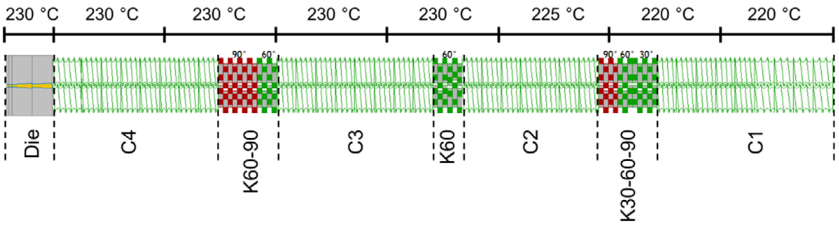

FIGURE 1 Screw profile in which the zones are delimited by dotted lines and identified by the corresponding assigned code. The temperature profile is also reported.

TABLE 1 Code, screw element characteristics, and length from the hopper to the die.

Code	Screw element	Length (mm)
C1	Conveying—pitch 7.5 mm	44.00
	Conveying—pitch 5.5 mm	55.00
K30-60-90	Kneading—angle 30°	13.75
	Kneading—angle 60°	8.25
	Kneading—angle 90°	11.00
C2	Conveying—pitch 5.5 mm	77.00
K60	Kneading—angle 60°	16.50
C3	Conveying—pitch 5.5 mm	88.00
K60-90	Kneading—angle 60°	11.00
	Kneading—angle 90°	22.00
C4	Conveying—pitch 5.5 mm	77.00
	Conveying—pitch 6 mm	16.50

the second conveying section. Considering the kneading elements, they are identified with the letter "K" and one or more numbers referring to the stagger angle between the disks. As an example, "K60-90" indicates the kneading section in which the stagger angle is 60° for the element in the first part and 90° in the following. The temperature profile is reported in Figure 1 and was maintained constant. Also, the flow rate was kept at 290 g/h, while the screw speed was alternatively 150 or 300 rpm.

Different blends characterized by a different HV to LV content were produced. In particular, the HV:LV wt% ratio was fixed at: 100:0, 70:30, 50:50, 30:70, and 0:100. The pellets were weighed and tumbled before being placed in the hopper, and after compounding, the materials were cooled in a water tank and granulated. The polymers were dried overnight in a vacuum oven at 80°C before processing.

The obtained materials were named after the HV content and the screw speed. For instance, "30HV_150rpm" refers to the material containing 30 wt% of HV, 70 wt% of LV, and processed at 150 rpm.

A Collin P200 T (Maitenbeth, Germany) was exploited for the hot compression molding production of the specimens for rheological analyses. The materials were maintained at 230°C for 3 min and 50 bar.

2.2.2 | Characterization

Rheological analyses were carried out with a strain-controlled ARES rheometer (TA Instruments—New Castle, DE, USA). A parallel plate—plate 25 mm geometry was maintained with a gap of 1 mm during the tests. The frequency sweep measurements were performed at 250°C under a nitrogen atmosphere with a frequency ranging from 100 rad/s to 0.1 rad/s. The strain amplitude was selected within the linear viscoelastic region for all samples (preliminarily determined through strain sweep tests).

DSC Q20 (TA Instrument—New Castle, DE, USA) was exploited for the thermal characterizations. The samples having a mass of 7 ± 1 mg were subjected to two heating scans from 0 to 250°C, separated by a cooling scan from 250 to 0°C. The heating and cooling ramps were carried out at 10°C/min. A flow of 50 mL/min nitrogen purged the chamber. The melting enthalpy (ΔH_m) was calculated as the integral of the multiple melting peaks in the second heating ramp. The crystallinity was estimated by considering 230 J/g[30] as the melting enthalpy of the completely crystalline PA6. Besides, the Peak Deconvolution tool of Origin 2020 was exploited to perform the deconvolution of the multiple peaks, aiming at identifying the content of α and γ crystalline phases in the second heating ramp. The Gaussian distribution was chosen as the fitting function, and the height of the peak was exploited as indicative of the crystallinity content.[30,44,55,56] In addition, the α/γ height ratio was calculated as the ratio between the two deconvoluted peak heights.

Besides, the crystallization temperature (T_{cryst}), corresponding to the peak temperature in the cooling ramp, was evaluated.

2.2.3 | Compounding modeling

The compounding processing was simulated with Ludovic® (version 7.1). The software exploits a local one-dimensional approach, allowing for modeling the melt flow in the direction parallel to the screws of an intermeshing co-rotating twin-screw extruder under

stationary conditions. As a result, process parameters such as shear rate, temperature, and residence time are obtained.[57–62]

Some inputs are required to perform the simulation. In particular, the screw profile, the temperature profile, the feed rate, the screw speed, and the thermal and rheological characteristics of the materials.[57] The simulations were carried out considering the processing conditions described in Section 2.2.1. Besides, the thermal characteristics of the materials required by the software were evaluated through DSC analyses, while the rheological data were obtained by performing frequency sweep tests at three different temperatures (namely, 230, 240, and 250°C).

3 | RESULTS

3.1 | Ludovic® simulation

The shear rate (s^{-1}), temperature (°C), total residence time (TRT, s) and local residence time (LRT, s) along the screws were modeled and will be discussed in consideration of the variation of the screw speed and the HV content in the blends.

Figure 2 depicts the trend of the shear rate and the TRT. The reported curves are representative of all the evaluated materials because no variation related to the different M_W or M_W distribution emerged from the simulations. Focusing on the first parameter, it can be appreciated that it is characterized by a minimum in correspondence to the conveying zones and a maximum reached in the kneading sections. Specifically, at 300 rpm, the two values are 80 and 152 s^{-1}, while at 150 rpm, they are 40 and 76 s^{-1}. Thus, the shear rate is determined from both the screw elements and the screw speed.

On the other hand, the TRT corresponds to the time spent by the material from the hopper to the die and can also be considered as the sum of the LRTs required to go along each kneading or conveying section (Table S1). As can be observed from the data reported in Figure 2, at 150 rpm, the TRT increases by 25% compared to the value obtained for 300 rpm. Besides, the enhancement is related only to the increase of the LRT in the conveying elements, which is almost doubled. In fact, no variation in the LRT along the kneading sections emerges. So, as already observed for the shear rate, the TRT also depends only on the screw speed, to which it is related by an inverse relationship, and on the screw elements.

Then, considering the trend of the temperature along the screw profile, a common behavior of this parameter can be observed, despite the considered formulation and screw speed (Figure 3). Specifically, higher values were obtained in correspondence with the kneading elements, where a larger heating rate corresponds to the higher stagger angles. On the other hand, the temperature decreases along the conveying zones. In all the cases, the maximum temperature is reached at the end of K60-90. Besides, in Figure 3 it can be observed that, considering a specific formulation, the values at 300 rpm are always higher than those at 150 rpm. In addition, the increase in temperature is associated with the higher HV content at a certain screw speed. These results indicate that the screw profile, the screw speed, and the material viscosity play an important role in determining the actual temperature. In particular, the increase in the content of HV

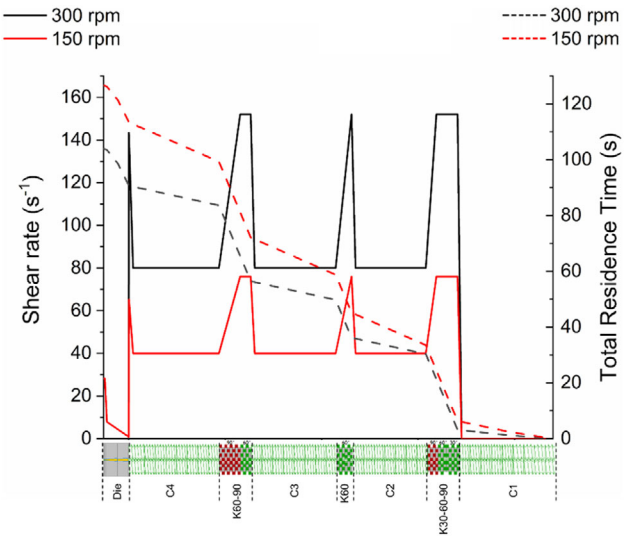

FIGURE 2 Shear rate and total residence time along the screw profile.

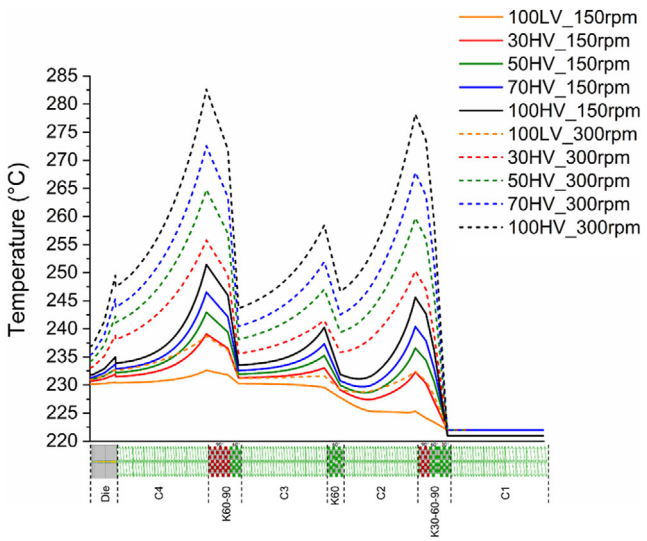

FIGURE 3 Temperature profiles along the screws.

and/or the screw speed results in the enhancement of the overall temperature profile along the screws. The actual maximum and minimum temperatures faced in each screw section are reported in Tables S2 and S3.

Owing to the Ludovic® simulation, the evolution of the thermo-mechanical history experienced by the materials was provided and discussed as a function of the screw speed and the blend composition. The impact of the variation of temperature, shear rate, and residence time on the rheological behavior and final microstructure of the blends will be discussed in the following.

3.2 | Rheology

The complex viscosity (η^*) of the materials as a function of the frequency is reported in Figure 4. Concerning the matrices, as expected considering their different M_W,[63–66] 100 HV shows higher values as compared to 100 LV. Besides, both materials are characterized by a non-Newtonian behavior in the low-frequency region, likely due to the presence of H-bonding that prevents a complete relaxation of the macromolecules.[1,2,7,8,37,65,67] In addition, from the comparison of the complex viscosity curves of the two materials processed at 150 or 300 rpm, a very similar rheological behavior is observed. Therefore, for the neat matrices, the rheological behavior remains largely unaffected by the screw speed value. Considering the blends, the complex viscosity increases with increasing HV content; besides, the values are distributed between those of the two matrices according to their relative content. Furthermore, a slight non-Newtonian behavior at low frequencies can be noticed. As above discussed in the case of the matrices, this feature can be related to the presence of the H-bonding between the macromolecules, slowing down the relaxation dynamics. Additionally, also for the blends, the value of the screw speed has a negligible effect on the complex viscosity trend, indicating that the blend formulation (i.e., the HV:LV ratio) has a predominant effect over the screw speed in determining their complex viscosity.

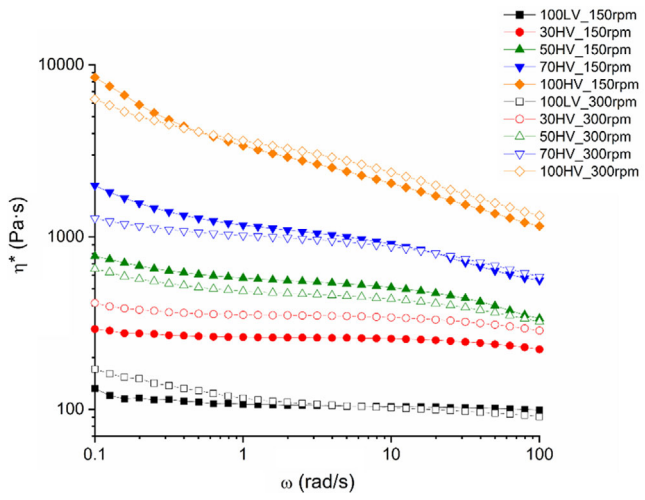

FIGURE 4 Complex viscosity of all investigated materials.

3.3 | DSC

The thermograms collected during the second heating scans are reported in Figure 5A–C. Looking at the pre-processing materials (Figure 5A), both LV and HV show a peak at 222°C, attributable to the α crystalline phase.[30] Besides, pre-processing HV also presents a shoulder at lower temperatures, indicating the presence of a low amount of γ crystalline phase in this sample.[44,68] According to Cavallo et al.[33] the presence of the γ crystalline phase only in the polymer having high M_W can be explained by considering that the stability interval of this phase in PA6 is related to the M_W. In particular, it was demonstrated that the range of stability of the γ phase increases in correspondence with higher M_Ws.[33]

On the other hand, when comparing such data with the second heating ramp of the two polymers processed at 150 or 300 rpm (Figure 5B,C), the presence of a multiple peak can be clearly observed. More specifically, two different peaks were identified through a deconvolution procedure (the melting temperatures are reported in Table S4) and attributed to the γ and α crystalline phases, respectively. Furthermore, the same multiple peak was observed for all the blends. Therefore, firstly, it emerged that the compounding process promotes the formation of the γ phase in PA6 despite the screw speed, HV content, and M_W distribution. Furthermore, considering the thermograms collected during the cooling scan (Figure 5D,E), a single peak (crystallization temperatures reported in Table S5) is observed for all the investigated materials, irrespective of the screw speed and the blend formulation.[30,68]

In Figure 6A, the values of ΔH_m recorded during the second heating ramp are reported as a function of the HV content. As expected, despite the screw speed considered, for the two matrices, the value decreases with the increase of the M_W.[69] Focusing on the starting PAs, higher ΔH_m values were obtained for the processed polymers as compared to the pre-processed ones. Additionally, the value increases with the screw speed, and the effect is more pronounced for HV. On the other hand, when considering the blends, two different trends are distinguished depending on the screw speed. In fact, when the materials were processed at 150 rpm, the three melting enthalpies follow a decreasing linear trend with the increase of the HV content, and the values are higher than those expected

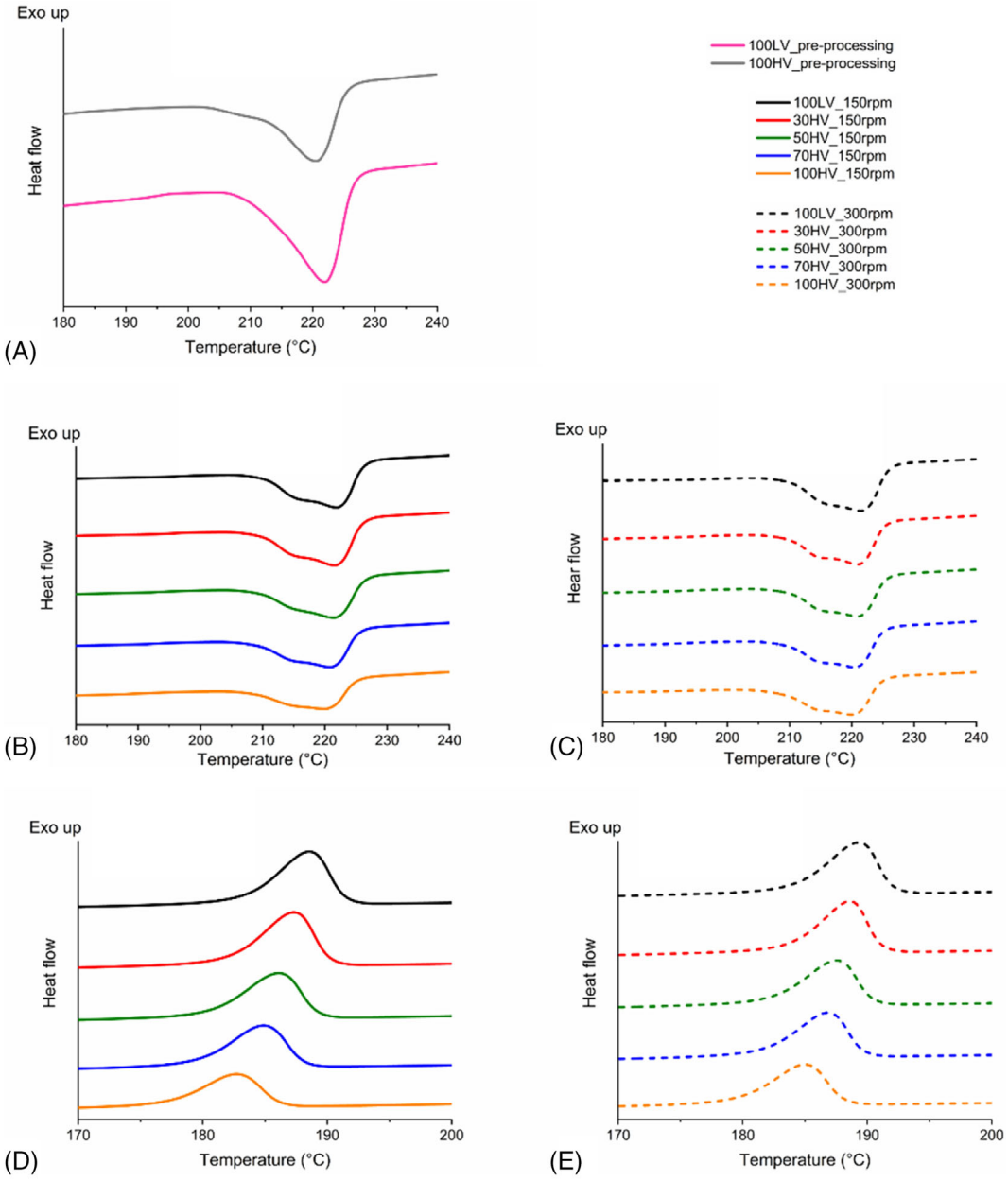

FIGURE 5 Heating thermograms recorded during the second heating scan for (A) 100LV and 100HV before processing and for the materials compounded at (B) 150 rpm and (C) 300 rpm; cooling ramps of for the materials produced at (D) 150 rpm and (E) 300 rpm. HV, high viscosity polymer; LV, low viscosity polymer.

according to the calculated linear combination of the ΔH_m of 100LV_150 rpm and 100HV_150 rpm (dotted line in the graph). At variance, for the blends processed at 300 rpm, the melting enthalpy at the second heating ramp is practically independent from the HV content, which seems not to affect the final crystallinity. Also, the values are lower than those expected from the calculation through a linear combination rule.

Further considerations emerge from the comparison of the data for the blends processed at different screw speeds. In fact, though higher ΔH_m were recorded for materials processed at 150 rpm, the difference with the value of the corresponding systems processed at 300 rpm lowers with increasing HV content. Therefore, in the case of the matrices, the screw speed and M_W have an independent effect on the final crystallinity content, while this feature is no longer verified for the blends. The crystallinity content of the matrices and the blends processed at 150 and 300 rpm, along with those of the pre-processed polymers, is reported in Table S6.

Besides, in Figure 6B, the values of the crystallization temperatures are reported. As far as the matrices are

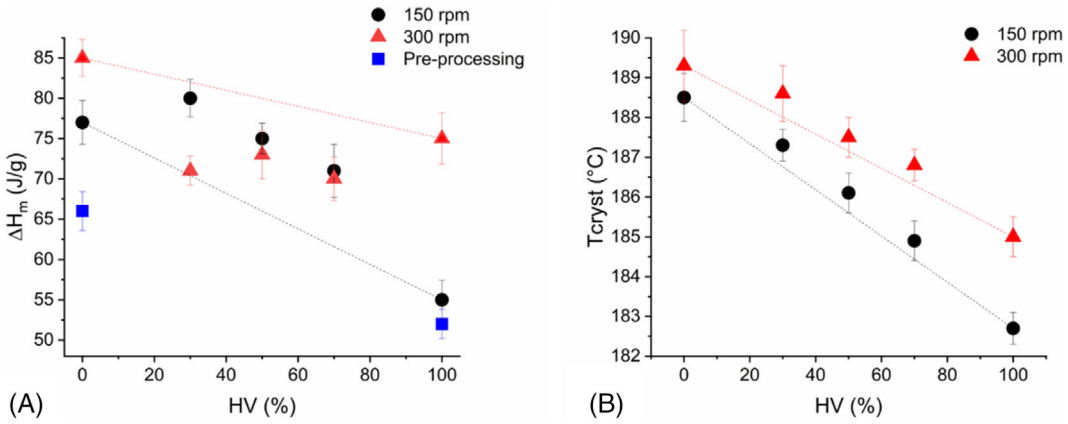

FIGURE 6 (A) ΔH_m evaluated at the second heating ramp for the materials processed at 150 or 300 rpm and pre-processed (the dotted lines represent the linear composition of the ΔH_m of the two matrices); (B) crystallization temperature for all the investigated materials (the linear composition of T_{cryst} of the two matrices is reported as dotted line). HV, high viscosity polymer.

concerned, T_{cryst} decreases with increasing the HV content, according to the literature,[9,70] and the trend is independent of the screw speed considered. The same behavior is appreciated for the blends, for which (regardless the screw speed) the experimental T_{cryst} is quite in accordance with the linear combination of the crystallization temperatures (represented by the dotted lines) of the matrices, notwithstanding the experimental values being higher than the calculated ones. In addition, considering the T_{cryst} of a single material at the two different screw speeds, higher values are obtained for the processing at 300 rpm, suggesting that the increase of the parameter positively affects the T_{cryst}, regardless of HV content.

Owing to a deconvolution procedure, the analysis of the α and γ crystalline phases content was performed. Figure 7 a and b report the height of the peaks relative to α and γ phases for the material processed at 150 and 300 rpm, respectively. Focusing on the matrices, at both screw speeds, the α phase is the more abundant, and the content of the two crystalline species is higher for 100LV than for 100HV. In addition, when comparing the peak height of the processed matrices with the pre-processing ones, some considerations can be made. Specifically, in LV, the α phase content before compounding is higher than that after processing, despite the screw speed; otherwise, for 100 HV processed at 300 rpm, the value is comparable with that of the pre-processed material. On the other hand, the γ phase content in the pre-processing HV is lower as compared to 100HV_150rpm and 100HV_300rpm. Therefore, it is confirmed that the compounding process promotes the formation of γ phase, in accordance with the observations relative to Figure 5. Also, considering the blends (Figure 7A,B), the predominance of α over γ can be appreciated, along with a decreasing trend with the increase of the HV content.

Besides, a more refined analysis of the effect of the variables on the reciprocal phase content emerges when looking at the α/γ ratio (Figure 7C). In fact, for both 100LV and 100HV, the larger α/γ is reached when the materials are processed at 300 rpm, indicating that the formation of the α phase is promoted at high screw speed. On the other hand, a different trend is observed for the blends. In fact, only 70HV has a behavior comparable to that of the matrices, while for 30HV and 50HV, the higher α/γ was achieved at 150 rpm. Besides, focusing on the α/γ ratio of the blends clearly reveals the interdependence of the effect of screw speed and M_W. As a result, the same α/γ ratio can be obtained with different combinations of parameters. For instance, 30HV_150rpm, 50HV_300rpm, and 70HV_300rpm are characterized by a comparable α/γ value.

4 | DISCUSSION

In the previous section, the results relative to the effect of the variation of the screw speed and HV content on the processing temperature, shear rate, and residence time of the materials have been commented on, along with the data coming from rheological and thermal characterizations. Hereafter, the relationships between the results of the Ludovic® simulations and the materials' characteristics will be discussed, taking particularly into consideration the role of the thermo-mechanical field in affecting the H-bonding and the following implications.

4.1 | Matrices

Firstly, the effect of the variation of the screw speed and M_W will be assessed. Considering the melting enthalpies

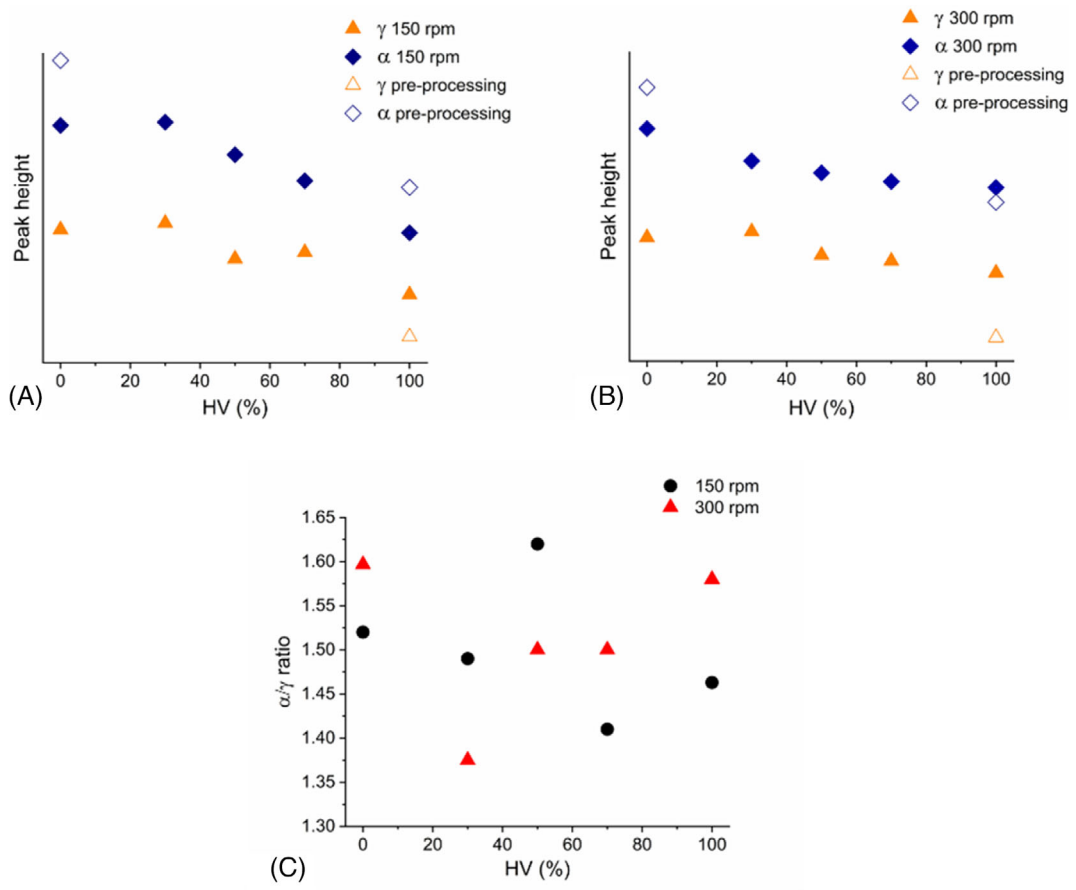

FIGURE 7 Height of α and γ peaks obtained from the deconvolution of the multiple peak of the materials produced at (A) 150 rpm or (B) 300 rpm and (C) corresponding α/γ height ratio. Also, in (A) and (B), the comparison with the pre-processing values is reported. HV, high viscosity polymer.

of the materials before and after the processing, higher values were obtained in the latter case. This behavior is in accordance with previous results reported in the literature on PAs and is related to the larger molecular ordering resulting from the applied shear during melt blending. Specifically, the phenomenon is due to the action of FIC and the presence of H-bonding.[7,18,19,29,71,72] Concerning the processed materials, the results of the DSC analyses showed that the processing at 300 rpm (hence, as demonstrated by Ludovic® simulations (Figure 2), at high shear rate) promotes the obtainment of higher melting enthalpy values. Therefore, according to the literature,[73] a relation between the applied shear rate and the resulting crystalline content was verified.

On the other hand, it is known that different shear-induced crystallization regimes, promoting different microstructural evolutions, can be distinguished depending on the macromolecular characteristics of the polymer and the applied shear rate.[19,42,72,74] In order to evaluate which regime is active, the two Weissenberg numbers were exploited. These parameters are the product of the applied shear rate and the longest relaxation time (W_{rep}) and the Rouse time (W_s), respectively. In particular, W_{rep} is related to the orientation of the chains while W_s is related to the stretching of the macromolecules. At low shear rates, where both W_{rep} and W_s are lower than one, a poor or negligible effect on the crystallinity content is expected, and the final morphology is comparable to that obtained in a quiescent state. When $W_{rep} > 1$ and $W_s < 1$, the enhancement in the crystallization kinetics, along with the improved orientation, drives a fine spherulites microstructure with more ordered chains. Lastly, at high shear rates, the value of both W_{rep} and W_s is above one and the macromolecules are stretched. In this last case, the evolution of the system may ultimately result in the formation of shish-kebab crystalline structures.

In the present study, W_{rep} and W_s were calculated for 100HV and 100LV processed at 150 and 300 rpm using the shear rate values obtained with Ludovic® simulation and the values of the longest relaxation time and Rouse time calculated by Massaro et al.[42] In all cases, $W_{rep} > 1$ and $W_s < 1$ (Table S7) were obtained, indicating an active FIC regime such that a morphology characterized by fine spherulites containing ordered chains is expected.

Besides, the above results highlight the antagonistic role of the memory effect and FIC. Specifically, 100HV is characterized by a larger content of intramolecular H bonding and entanglement as compared to 100LV, due to its higher M_W. As a result, the molecular friction in the melt state is higher and the motion of the chains is restricted, causing the obtainment of lower crystallinity content compared to 100LV.[2,17,75] On the other hand, the smaller difference between the ΔH_m of the two matrices processed at 300 rpm with respect to the corresponding values of 100LV_150rpm and 100HV_150rpm (Figure 6A) can be explained by considering the actual temperatures reached by the materials along the screws. In fact, the Ludovic® simulations (Figure 3) highlighted that 100 HV is subjected to higher temperatures than 100LV processed in the same conditions, and the temperature differences are particularly emphasized at 300 rpm. Therefore, the larger values may have an effect on the stability of intermolecular H-bonding. In particular, it is well known that the hydrogen bonding in PAs reaches a dynamic temperature-dependent equilibrium in the molten state, notwithstanding the decrease of the density of bindings with the increase of the temperature. Specifically, the erasing of the memory effect for PA6 is still a debated topic, and at least two different temperature–time combinations can be found in the literature, which are 270°C for 10 min or 280°C for 90 min.[2,8,13,15] Considering all the above, the lower difference between the ΔH_m of 100LV_300rpm and 100HV_300rpm may be explained by the decrease of the memory effect intensity due to the higher temperatures reached when the processing is carried out at 300 rpm. In fact, the reduction of the intermolecular H-bonding density results in a less intense molecular friction and improved chain mobility.[2] Also, the entanglements decrease with the increased screw speed.[17] As a consequence, a lower memory effect would be expected in opposition to the FIC. This argument would also support the data relative to the α/γ ratio. As appreciated in Figure 7C, the ratios for 100HV and 100LV have much closer values when processed at 300 instead of 150 rpm. In accordance with the above, this may be related to a more similar effect of the shear on the microstructural organization of 100HV_300rpm and 100LV_300rpm due to the lower density of molecular constraints.

As a result, as the screw speed increases, the impact of FIC tends to become predominant over the memory effect. Nevertheless, the latter has to be considered still active even in the processing of 100HV_300rpm due to several reasons.[2,13,17] Firstly, the TRT at the higher screw speed is 104 s (Figure 2), which is lower than the time needed to erase the memory effect according to the literature.[2,8,13,15] Besides, even if the reported peak temperature is higher than the minimum critical temperature of 270°C, the average value faced by the material during processing is lower. Lastly, the role of the entanglement in promoting the memory effect has to be taken into account because its presence is confirmed by the non-Newtonian behavior characterizing the complex viscosity of 100HV_300rpm at low frequencies (Figure 4). On the other hand, even if the H-bonding favors the FIC, the phenomenon is less affected by the negative impact of the temperature because it is promoted by the increase of the shear rate, as emerged from the enhancement of W_{rep} from 150 to 300 rpm (Table S7). This is confirmed by the T_{cryst} data (Figure 6B). In fact, the materials processed at 300 rpm are characterized by higher values. As documented in the literature, a larger crystallization kinetic is associated with a larger crystallization temperature.[9,19,71,76] In particular, the higher increase is appreciated for 100HV, and this can be interpreted as a further confirmation of the predominant role of FIC over the memory effect in such material processed at 300 rpm.

Further considerations can be referred to the effect of the screw speed on the microstructure. From the comparison of the α and γ content before and after the processing, the decrease of the first and the increase of the latter emerged (Figure 5 and Figure 7). Taking into account that α is the most stable crystalline phase,[30] such evolution of the morphology suggests a decrease in the chain ordering due to the compounding. Besides, the increase of the α/γ ratio for both 100LV and 100HV when processed at 300 rpm instead of 150 rpm (Figure 7C) evidences the opposite trend with the increase of the screw speed. Accordingly, the role of high shear rate values in promoting the formation of the α crystalline phase while negligibly affecting the γ content was reported for PA66.[73]

The formation of the less stable γ phase with processing can be explained by considering the opposition of the memory effect to the FIC. In fact, the presence of the molecular constraints at 150 rpm hinders the mobility of the macromolecules and, thus, the achievement of the conformation typical of the α phase. On the other hand, the increase of the screw speed to 300 rpm lowers the H-bonding and entanglements; thus, the larger content in the α phase is promoted by the higher chain mobility.

In conclusion, in the processing of the matrices, the crystallinity content and the α/γ ratio are promoted by the increase of the screw speed, while a minor impact is attributed to the M_W. Besides, the effect of the M_W appears to be related to the screw speed considered.

4.2 | Blends

When focusing on the blends, for the materials processed at 150 rpm, the observed decreasing trend of the ΔH_m

with increasing HV content (Figure 6A) can be explained by considering the antagonism of the memory effect and the FIC. In fact, the increase in HV content induces a more pronounced memory effect due to the presence of high M_W macromolecules and the consequent increase in the molecular constraints (as also testified to and confirmed by the non-Newtonian behavior in the low-frequency region) (Figure 4). On the other hand, the experimental values of ΔH_m show a positive deviation from the linear combination of the melting enthalpies of the two matrices. This would suggest the presence of a cooperative mechanism active in the presence of the bimodal M_W distribution, which results in the promotion of crystallinity.

Then, referring to the blends processed at 300 rpm, the increase in the screw speed negatively affects the crystallinity. In fact, the experimental data are lower than the values calculated in accordance with the linear combination law and are quite unaffected by the HV content. Besides, the α/γ ratio is greatly affected by the presence of both LV and HV in the formulation, and the resulting values are always lower than those of the two matrices (Figure 7C). Therefore, it appears that the increase in the screw speed promotes chain disorder.

On top of that, from the comparison of the T_{cryst} (Figure 6B), the crystallization kinetic in the blends processed at 300 rpm is expected to be higher than those of the materials obtained at 150 rpm.[9,19,71,76]

In conclusion, in the blends cannot be clearly understood, the effect of the variation of the screw speed and HV content cannot be clearly understood separately. In fact, the experimental results suggest an interdependence of the impact of the two parameters on the microstructure. Furthermore, the theories modeling the FIC do not describe the transition morphologies and, in most cases, do not consider the contribution of the non-crystalline ordered phase to the formation of stable nuclei.[19]

5 | CONCLUSIONS

In the present study, the processing parameter–microstructure relationships in melt-compounded PA6 having different viscosities were investigated, specifically focusing on the effect of the variation of screw speed and M_W. The simulation of the thermo-mechanical field performed with the Ludovic® software highlighted the role of the screw speed in increasing the shear rate and decreasing the TRT. Besides, the simulations showed that the actual temperature along the screws increases with increasing the material M_W or the screw speed. The thermal characterization of the formulated materials demonstrated the increase of both the overall crystallinity and the α/γ content with increasing the screw speed due to the antagonistic role of the FIC and memory effect. Besides, it was assessed that the intensity of the two phenomena was dependent on the shear rate and temperature faced by the material during processing. In particular, the increase of the shear rate reduced the entanglement density, while the increase of the temperature lowered the H-bonding density. As a result, the macromolecular constraints were reduced, and the impact of the FIC was predominant over the memory effect. For this reason, the overall crystallinity, as well as the content of the more stable α crystalline phase, increased. Finally, blends characterized by different HV:LV ratios were formulated and the rheological and thermal characteristics analyzed, assessing the interdependency of the effect of the variation of the screw speed and viscosity on the resulting crystallinity content.

ACKNOWLEDGMENT

Open access publishing facilitated by Politecnico di Torino, as part of the Wiley - CRUI-CARE agreement.

DATA AVAILABILITY STATEMENT

The data that support the findings of this study are available from the corresponding author upon reasonable request.

ORCID

Fulvia Cravero https://orcid.org/0000-0002-3699-7370
Rossella Arrigo https://orcid.org/0000-0002-0291-2519

REFERENCES

1. Murthy NS. Hydrogen bonding, mobility, and structural transitions in aliphatic polyamides. *J Polym Sci B*. 2006;44(13):1763-1782. doi:10.1002/polb.20833
2. Seguela R. Overview and critical survey of polyamide6 structural habits: misconceptions and controversies. *J Polym Sci*. 2020;58(21):2971-3003. doi:10.1002/pol.20200454
3. Lee JK, Lim HS. Movement, wear comfort, and compression evaluation of nylon and polyurethane blend stretch knit material and 3D virtual fitting stress strain comparison. *Fibers Polym*. 2023;24(7):2541-2555. doi:10.1007/s12221-023-00246-0
4. Rodríguez MP, Vázquez-Vélez E, Martinez H, Torres-Islas A. Life cycle analysis of a novel process from the automotive industry in Mexico for recycling nylon 6,6 into polymeric coatings. *Sustainability*. 2023;15(12):9810. doi:10.3390/su15129810
5. Guo A, Liu C, Li S, et al. Water absorption rates and mechanical properties of material extrusion-printed continuous carbon fiber-reinforced nylon composites. *J Mater Res Technol*. 2022;21:3098-3112. doi:10.1016/j.jmrt.2022.10.134
6. Shakiba M, Rezvani Ghomi E, Khosravi F, et al. Nylon—a material introduction and overview for biomedical applications. *Polym Adv Technol*. 2021;32(9):3368-3383. doi:10.1002/pat.5372
7. Khanna YP, Kumar R, Reimschuessel AC. Memory effects in polymers. III. Processing history vs. crystallization rate of nylon

6—comments on the origin of memory effect. *Polym Eng Sci*. 1988;28(24):1607-1611. doi:10.1002/pen.760282406
8. Liu X, Wang Y, Wang Z, et al. The origin of memory effects in the crystallization of polyamides: role of hydrogen bonding. *Polymer*. 2020;188:122117. doi:10.1016/j.polymer.2019.122117
9. Fornes TD, Paul DR. Crystallization behavior of nylon 6 nanocomposites. *Polymer*. 2003;44(14):3945-3961. doi:10.1016/S0032-3861(03)00344-6
10. Garcia D, Starkweather HW. Hydrogen bonding in nylon 66 and model compounds. *J Polym Sci Polym Phys Ed*. 1985;23(3):537-555. doi:10.1002/pol.1985.180230310
11. Ma GQ, Sun ZB, Ren JY, et al. Reorganization of hydrogen bonding in biobased polyamide 5,13 under the thermo-mechanical field: hierarchical microstructure evolution and achieving excellent mechanical performance. *Biomacromolecules*. 2022;23(9):3990-4003. doi:10.1021/acs.biomac.2c00826
12. Wang Z, Lin N, Kang H, Hao X, Liu R. Isodimorphism in polyamide 56/polyamide 66 blends with controllable thermal and mechanical properties. *ACS Appl Polym Mater*. 2022;4(12):9407-9416. doi:10.1021/acsapm.2c01683
13. Avramova N, Fakirov S. Cumulative erasing effect in the melt memory of nylon 6. *J Polym Sci B*. 1986;24:761-768. doi:10.1002/polb.1986.090240403
14. Murthy NS, Stamm M, Sibilia JP, Krimm S. Structural changes accompanying hydration in nylon 6. *Macromolecules*. 1989;22:1261-1267. doi:10.1021/ma00193a043
15. Schroeder LR, Cooper SL. Hydrogen bonding in polyamides. *J Appl Phys*. 1976;47(10):4310-4317. doi:10.1063/1.322432
16. Skrovanek DJ, Painter PC, Coleman MM. Hydrogen bonding in polymers. 2. Infrared temperature studies of nylon 11. *Macromolecules*. 1986;19(26):1002. doi:10.1021/ma00157a037
17. Sangroniz L, Müller AJ, Cavallo D. Origin of melt memory effects in poly(ethylene oxide): the crucial role of entanglements. *Macromol Rapid Commun*. 2024;45(12):e2400011. doi:10.1002/marc.202400011
18. Jariyavidyanont K, Mallardo S, Cerruti P, et al. Shear-induced crystallization of polyamide 11. *Rheol Acta*. 2021;60(5):231-240. doi:10.1007/s00397-021-01264-6
19. Wang Z, Ma Z, Li L. Flow-induced crystallization of polymers: molecular and thermodynamic considerations. *Macromolecules*. 2016;49(5):1505-1517. doi:10.1021/acs.macromol.5b02688
20. Zhou W, Cui K, Tian N, et al. Disentanglement decelerating flow-induced nucleation. *Polymer*. 2013;54(2):942-947. doi:10.1016/j.polymer.2012.11.074
21. Zhu S, Wang Z, Su F, et al. The influence of inertia and elastic retraction on flow-induced crystallization of isotactic polypropylene. *J Rheol*. 2013;57(5):1281-1296. doi:10.1122/1.4812671
22. Courty S, Gornall JL, Terentjev EM. Induced helicity in biopolymer networks under stress. *Proc Natl Acad Sci USA*. 2005;102(38):13457-13460. doi:10.1073/pnas.0506864102
23. Olmsted PD, Poon WCK, Mcleish TCB, Terrill NJ, Ryan AJ. Spinodal-assisted crystallization in polymer melts. *Phys Rev Lett*. 1998;81(2):373-376. doi:10.1103/PhysRevLett.81.373
24. Shimada T, Doi M, Okano K. Concentration fluctuation of stiff polymers. III. Spinodal decomposition. *J Chem Phys*. 1988;88(11):7181-7186. doi:10.1063/1.454370
25. Doi M, Shimada T, Okano K. Concentration fluctuation of stiff polymers. II. Dynamical structure factor of rod-like polymers in the isotropic phase. *J Chem Phys*. 1988;88(6):4070-4075. doi:10.1063/1.453861
26. Liu D, Tian N, Huang N, et al. Extension-induced nucleation under near-equilibrium conditions: the mechanism on the transition from point nucleus to shish. *Macromolecules*. 2014;47(19):6813-6823. doi:10.1021/ma501482w
27. Ziabicki A, Alfonso GC. A simple model of flow-induced crystallization memory. *Macromol Symp*. 2002;185:211-231.
28. Roozemond PC, Peters GWM. Flow-enhanced nucleation of poly(1-butene): model application to short-term and continuous shear and extensional flow. *J Rheol*. 2013;57(6):1633-1653. doi:10.1122/1.4821609
29. Roozemond PC, Steenbakkers RJA, Peters GWM. A model for flow-enhanced nucleation based on fibrillar dormant precursors. *Macromol Theory Simul*. 2011;20(2):93-109. doi:10.1002/mats.201000059
30. Vanden Poel G, Mathot VBF. High performance differential scanning calorimetry (HPer DSC): a powerful analytical tool for the study of the metastability of polymers. *Thermochim Acta*. 2007;461(1–2):107-121. doi:10.1016/j.tca.2007.04.009
31. Khanna YP, Reimschuessel AC. Memory effects in polymers. I. Orientational memory in the molten state; its relationship to polymer structure and influence on recrystallization rate and morphology. *J Appl Polym Sci*. 1988;35:2259-2268. doi:10.1002/app.1988.070350824
32. Lotz B. Original crystal structures of even-even polyamides made of pleated and rippled sheets. *Macromolecules*. 2021;54(2):551-564. doi:10.1021/acs.macromol.0c02404
33. Cavallo D, Gardella L, Alfonso GC, Portale G, Balzano L, Androsch R. Effect of cooling rate on the crystal/mesophase polymorphism of polyamide 6. *Colloid Polym Sci*. 2011;289(9):1073-1079. doi:10.1007/s00396-011-2428-6
34. Kyotani M, Mitsuhashi S. Studies on crystalline forms of nylon 6. II. Crystallization from the melt. *J Polym Sci Part A*. 1972;2:1497-1508. doi:10.1002/pol.1972.160100807
35. Mileva D, Kolesov I, Androsch R. Morphology of cold-crystallized polyamide 6. *Colloid Polym Sci*. 2012;290(10):971-978. doi:10.1007/s00396-012-2657-3
36. Penel-Pierron L, Depecker C, Séguéla R, Lefebvre JM. Structural and mechanical behavior of nylon 6 films: part I. Identification and stability of the crystalline phases. *J Polym Sci B*. 2001;39(5):484-495. doi:10.1002/1099-0488(20010301)39:53.0.CO;2-R
37. Mayoral B, Harkin-Jones E, Khanam PN, et al. Melt processing and characterisation of polyamide 6/graphene nanoplatelet composites. *RSC Adv*. 2015;5(65):52395-52409. doi:10.1039/c5ra08509h
38. Wang L, Dong X, Huang M, Wang D. Transient microstructure in long alkane segment polyamide: deformation mechanism and its temperature dependence. *Polymer*. 2016;97:217-225. doi:10.1016/j.polymer.2016.05.038
39. Cai Z, Liu X, Zhou Q, et al. The structure evolution of polyamide 1212 after stretched at different temperatures and its correlation with mechanical properties. *Polymer*. 2017;117:249-258. doi:10.1016/j.polymer.2017.04.037
40. Thyashan N, Perera YS, Xiao R, Abeykoon C. Investigation of the effect of materials and processing conditions in twin-screw extrusion. *Int J Lightweight Mater Manuf*. 2024;7(3):353-361. doi:10.1016/j.ijlmm.2023.09.003
41. Furushima Y, Nakada M, Ishikiriyama K, et al. Two crystal populations with different melting/reorganization kinetics of isothermally crystallized polyamide 6. *J Polym Sci B*. 2016;54(20):2126-2138. doi:10.1002/polb.24123

42. Massaro R, Roozemond P, Van Puyvelde P. Flow-induced crystallization of polyamide-6. *Int Polym Process*. 2018;XXXIII(3):327-335. doi:10.3139/217.3524
43. Skorupska M, Kulczyk M, Przybysz S, Skiba J, Mizeracki J, Ryszkowska J. Mechanical reinforcement of polyamide 6 by cold hydrostatic extrusion. *Materials*. 2021;14(20):6045. doi:10.3390/ma14206045
44. Skorupska M, Kulczyk M, Denis P, Grzęda D, Czajka A, Ryszkowska J. Structural hierarchy of PA6 macromolecules after hydrostatic extrusion. *Materials*. 2023;16(9):3435. doi:10.3390/ma16093435
45. Parodi E, Peters GWM, Govaert LE. Structure-properties relations for polyamide 6, part 2: influence of processing conditions during injection moulding on deformation and failure kinetics. *Polymers*. 2018;10(7):779. doi:10.3390/polym10070779
46. Dencheva N, Denchev Z, Oliveira MJ, Funari SS. Relationship between crystalline structure and mechanical behavior in isotropic and oriented polyamide 6. *J Appl Polym Sci*. 2007;103(4):2242-2252. doi:10.1002/app.25250
47. Yan X, Imai Y, Shimamoto D, Hotta Y. Relationship study between crystal structure and thermal/mechanical properties of polyamide 6 reinforced and unreinforced by carbon fiber from macro and local view. *Polymer*. 2014;55(23):6186-6194. doi:10.1016/j.polymer.2014.09.052
48. Li C, Shan P, Soares JBP, Penlidis A. HDPE/LLDPE reactor blends with bimodal microstructures-part I: mechanical properties. *Polymer*. 2002;43(26):7345-7365. doi:10.1016/S0032-3861(02)00703-6
49. Long C, Dong Z, Wang K, Yu F, He C, Chen ZR. Molecular weight distribution shape approach for simultaneously enhancing the stiffness, ductility and strength of isotropic semicrystalline polymers based on linear unimodal and bimodal polyethylenes. *Polymer*. 2023;275:125936. doi:10.1016/j.polymer.2023.125936
50. Cravero F, Cavallini N, Arrigo R, Savorani F, Frache A. The effect of processing conditions on the microstructure of homopolymer high-density polyethylene blends: a multivariate approach. *Polymers*. 2024;16(7):870. doi:10.3390/polym16070870
51. Kim JH, Min BR, Kang YS. Thermodynamic model of the glass transition behavior for miscible polymer blends. *Macromolecules*. 2006;39(3):1297-1299. doi:10.1021/ma052436a
52. Wróblewska AA, Leoné N, De Wildeman SMA, Bernaerts KV. Towards high-performance materials based on carbohydrate-derived polyamide blends. *Polymers*. 2019;11(3):413. doi:10.3390/polym11030413
53. Wang L, Dong X, Huang M, Müller AJ, Wang D. The effect of microstructural evolution during deformation on the post-yielding behavior of self-associated polyamide blends. *Polymer*. 2017;117:231-242. doi:10.1016/j.polymer.2017.04.038
54. Cagiao ME, Ania F, Baltá Calleja FJ, Hirami M, Shimomura T. Structure-microhardness correlation in blends of nylon 6/nylon 66 monofilaments. *J Appl Polym Sci*. 2000;77(3):636-643. doi:10.1002/(SICI)1097-4628(20000718)77:33.0.CO;2-R
55. Yamamoto Y, Inoue Y, Onai T, Doshu C, Takahashi H, Uehara H. Deconvolution analyses of differential scanning calorimetry profiles of β-crystallized polypropylenes with synchronized X-ray measurements. *Macromolecules*. 2007;40(8):2745-2750. doi:10.1021/ma062784s
56. Gombás Á, Szabó-Révész P, Kata M, Regdon G, Erõs I. Quantitative determination of crystallinity of α-lactose monohydrate by DSC. *J Therm Anal Calorim*. 2002;68:503-510. doi:10.1023/A:1016039819247
57. Sciences Computers Consultants. *Ludovic® software*. Accessed February 1, 2024. https://www.scconsultants.com/en/ludovic-twin-screw-simulation-software.html
58. Castéran F, Ibanez R, Argerich C, Delage K, Chinesta F, Cassagnau P. Application of machine learning tools for the improvement of reactive extrusion simulation. *Macromol Mater Eng*. 2020;305(12):2000375. doi:10.1002/mame.202000375
59. Bernagozzi G, Arrigo R, Frache A. Evolution of the microstructure of PP-LDHs nanocomposites during melt compounding: a simulation approach. *Polymers*. 2023;16(1):70. doi:10.3390/polym16010070
60. Bochmann ES, Gryczke A, Wagner KG. Validation of model-based melt viscosity in hot-melt extrusion numerical simulation. *Pharmaceutics*. 2018;10(3):34-42. doi:10.3390/pharmaceutics10030132
61. Dubey S, Abhyankar H, Marchante V, et al. Modelling and validation of synthesis of poly lactic acid using an alternative energy source through a continuous reactive extrusion process. *Polymers*. 2016;8(4):164. doi:10.3390/polym8040164
62. Durin A, De Micheli P, Nguyen HC, David C, Valette R, Vergnes B. Comparison between 1D and 3D approaches for twin-screw extrusion simulation. *Int Polym Process XXIX*. 2014;5:641-648. doi:10.3139/217.2951
63. Porter RS, Johnson JF. The effect of molecular weight and distribution on polymer rheology near the entanglement region. *Trans Soc Rheol*. 1963;7(1):241-252. doi:10.1122/1.548955
64. Pearson GH, Garfield LJ. The effect of molecular weight and weight distribution upon polymer melt rheology. *Polym Eng Sci*. 1978;18(7):583-589.
65. Fornes TD, Yoon PJ, Keskkula H, Paul DR. Nylon 6 nanocomposites: the effect of matrix molecular weight. *Polymer*. 2001;42:9929-9940. doi:10.1016/S0032-3861(01)00552-3
66. Shi M, Wang L, Sun J, Yang W, Zhang H. Morphology and properties of polyolefin elastomer/polyamide 6/poly(lactic acid) in situ special-shaped microfibrillar composites: influence of viscosity ratio. *Polymers*. 2022;14(21):4556. doi:10.3390/polym14214556
67. Kiziltas A, Nazari B, Gardner DJ, Bousfield DW. Polyamide 6-cellulose composites: effect of cellulose composition on melt rheology and crystallization behavior. *Polym Eng Sci*. 2014;54(4):739-746. doi:10.1002/pen.23603
68. Tang J, Xu B, Xi Z, Pan X, Zhao L. Controllable crystallization behavior of nylon-6/66 copolymers based on regulating sequence distribution. *Ind Eng Chem Res*. 2018;57(44):15008-15019. doi:10.1021/acs.iecr.8b02671
69. Koyama K, Suryadevara J, Spuriell JE. Effect of molecular weight on high-speed melt spinning of nylon 6. *J Appl Polym Sci*. 1986;31(7):2203-2229. doi:10.1002/app.1986.070310723
70. Chivers RA, Moore DR. The effect of molecular weight and crystallinity on the mechanical properties of injection moulded poly(aryl-ether-ether-ketone) resin. *Polymer*. 1994;35(1):110-116. doi:10.1016/0032-3861(94)90057-4
71. Naudy S, David L, Rochas C, Fulchiron R. Shear induced crystallization of poly(m-xylylene adipamide) with and without nucleating additives. *Polymer*. 2007;48(11):3273-3285. doi:10.1016/j.polymer.2007.03.076
72. Housmans JW, Peters GWM, Meijer HEH. Flow-induced crystallization of propylene/ethylene random copolymers. *J Therm Anal Calorim*. 2009;98(3):693-705. doi:10.1007/s10973-009-0532-3
73. Rhoades AM, Gohn AM, Seo J, Androsch R, Colby RH. Sensitivity of polymer crystallization to shear at low and high

supercooling of the melt. *Macromolecules*. 2018;51(8):2785-2795. doi:10.1021/acs.macromol.8b00195

74. van Meerveld J, Peters GWM, Hütter M. Towards a rheological classification of flow induced crystallization experiments of polymer melts. *Rheol Acta*. 2004;44(2):119-134. doi:10.1007/s00397-004-0382-7
75. Sangroniz L, Meabe L, Basterretxea A, Sardon H, Müller AJ, Cavallo D. Chemical structure drives memory effects in the crystallization of homopolymers. *Macromolecules*. 2020;53(12):4874-4881. doi:10.1021/acs.macromol.0c00751
76. Khanna YP, Reimschuessel AC, Banerjie A, Altman C. Memory effects in polymers. II. Processing history vs. crystallization rate of nylon 6—observation of phenomenon and product behavior. *Polym Eng Sci*. 1988;28(24):1600-1606. doi:10.1002/pen.760282405

SUPPORTING INFORMATION

Additional supporting information can be found online in the Supporting Information section at the end of this article.

How to cite this article: Cravero F, Arrigo R, Frache A. Processing/microstructure relationships in melt compounded polyamide 6 with different molecular weights: Effect of screw speed and viscosity ratio. *Polym Eng Sci*. 2025;65(5):2525-2538. doi:10.1002/pen.27165